

A brighter era for silver chalcogenide semiconductor nanocrystals

Liyan Ming^{a,1}, Irene Zabala-Gutierrez^{b,1}, Oscar G. Calderon^c, Sonia Melle^c,
Erving Ximendes^{a,d}, Jorge Rubio-Retama^{b,d}, Riccardo Marin^{a,e,f,*}

^a Nanomaterials for BioImaging Group (nanoBIG), Departamento de Física de Materiales, Universidad Autónoma de Madrid, C/ Francisco Tomás y Valiente 7, 28049, Madrid, Spain

^b Departamento de Química en Ciencias Farmacéuticas, Universidad Complutense de Madrid, 28040, Madrid, Spain

^c Departamento de Óptica, Universidad Complutense de Madrid, 28037, Madrid, Spain

^d Nanomaterials for BioImaging Group (nanoBIG), Instituto Ramón y Cajal de Investigación Sanitaria IRYCIS, Ctra de Colmenar Km 9,300, 28034, Madrid, Spain

^e Institute for Advanced Research in Chemical Sciences (IAChem), Universidad Autónoma de Madrid, 28049, Madrid, Spain

^f Instituto de Ciencia de Materiales Nicolás Cabrera, Universidad Autónoma de Madrid, 28049, Madrid, Spain

ABSTRACT

Silver chalcogenide semiconductor nanocrystals (Ag₂E SNCs) have become a household name in the biomedical field, where they are used as contrast agents in bioimaging, photothermal therapy agents, and luminescent nanothermometers. The prominent position they have come to occupy in this field stems from a unique combination of features, above all near-infrared excitation and emission alongside low cytotoxicity. However, the first reports on Ag₂E SNCs showed that a great limitation of these luminescent nanomaterials resided in their low photoluminescence quantum yield, which results in reduced brightness: a crippling feature in bioimaging and biosensing. In this article, we provide an overview of the strategies developed to overcome this hurdle. These strategies aim to remedy the presence of defects in the SNC core and/or surface, the presence of metallic silver, and off-stoichiometric composition. These features stem from the high mobility and redox potential of Ag⁺ ions, alongside the difficulty in controlling the nucleation and growth rate of Ag₂E SNCs. The effectiveness of each approach is discussed. Lastly, a perspective on future research efforts to make Ag₂E SNCs even brighter – and thus more effective in biomedical applications – is provided, with the hope of inspiring further investigation on these nanomaterials with a rich, complex set of physicochemical and spectroscopic properties.

1. Introduction

Semiconductor nanocrystals (SNCs) have established themselves as reliable workhorses in the biomedical context for applications including bioimaging, biosensing, and cancer treatment [1–3]. The use of SNCs in this framework follows from a combination of physicochemical and spectroscopic properties, including adjustable surface chemistry and optical properties that can be finely tuned by selecting the SNC's size, composition, and core/shell architecture [4–7]. Thanks to these different “knobs” which one can modulate, SNCs can be prepared with strong, broadband photon absorption and photoluminescence spanning the UV-to-near infrared (NIR) spectral range. Regarding the working spectral range, NIR-operating luminescent nanoparticles – and hence SNCs among them – afford the best performance when bio-related applications are sought after. This is because within the so-called biological or optical windows (NIR-I, 750–950 nm; NIR-II, 1000–1350 nm; NIR-III, 1550–1800 nm) the biological tissues are more transparent to photons and less autofluorescence (i.e., the photoluminescence of

endogenous tissue components) is encountered [8,9].

In this frame of reference, silver chalcogenide (Ag₂E; E = S, Se, Te) SNCs emerge as ideal candidates for biomedical applications, owing to their benign chemical composition alongside optical absorption and emission in the NIR. Indeed, they have been successfully employed in whole-body imaging at the preclinical level, as well as for thermal sensing and imaging in animal models [10–14]. Overall, they represent the state-of-the-art as far as SNCs for biomedical applications working in the NIR are concerned. However, their performance in bioimaging and biosensing is inherently limited by their poor photoluminescence quantum yield (PLQY, the number of photons emitted per absorbed photon) [15]. Values below or around 1% are generally reported for Ag₂E SNCs dispersions in aqueous media: A far cry from the PLQY values of, e.g., PbS SNCs, which often exceed 30% [16–19]. Therefore, several strategies have been developed to tackle this issue, including control of the reactivity of the reaction mixture, composition control via cation exchange, and post-synthesis modification strategies (Fig. 1).

Herein, we provide a bird-eye view of the approaches proposed in the

* Corresponding author. Nanomaterials for BioImaging Group (nanoBIG), Departamento de Física de Materiales, Universidad Autónoma de Madrid, C/ Francisco Tomás y Valiente 7, 28049, Madrid, Spain.

E-mail address: riccardo.marin@uam.es (R. Marin).

¹ L. Ming and I. Zabala-Gutierrez contributed equally.

<https://doi.org/10.1016/j.optmat.2023.113940>

Received 2 March 2023; Received in revised form 4 May 2023; Accepted 22 May 2023

Available online 3 June 2023

0925-3467/© 2023 The Authors. Published by Elsevier B.V. This is an open access article under the CC BY license (<http://creativecommons.org/licenses/by/4.0/>).

literature to increase the PLQY value in Ag₂E SNCs. After an initial description of the general properties of Ag₂E SNCs, the different families of strategies are discussed in detail. Lastly, we give an outlook of what the future holds for Ag₂E SNCs in the biomedical context, also identifying hybrid strategies to improve the properties of these photoluminescent nanomaterials, and the fields that can benefit the most from this experimental effort. We should underscore that this manuscript is not a comprehensive review of the applications of Ag₂E SNCs in the biomedical context. The interested reader is encouraged to refer to reviews on Ag-based SNCs or, more generally, on NIR-active nanoparticles for bio-related applications [5,20,21].

2. General properties of Ag₂E SNCs and their relevance in biomedical applications

The appeal of Ag₂E SNCs in biomedical applications follows from a unique combination of properties. To begin with, these materials feature low cytotoxicity, thanks to the lack of highly poisonous elements of which other SNCs are composed (Hg, Cd, Pb), and to a low solubility product in water (e.g., $K_{sp}(\text{Ag}_2\text{S}) = 6.3 \cdot 10^{-50}$) [22], which stems concerns over the release of cytotoxic Ag⁺ ions in aqueous media [23,24]. Compared to another class of negligibly toxic SNCs, i.e., those made of InP [25], the synthesis of Ag₂E SNCs is more straightforward and does not entail the use of hazardous chemicals, making the scale-up of the synthesis more realistic and safer.

The most relevant features of Ag₂E are reported in Table 1, which includes the respective bulk band gap (E_g), Bohr radius (r_B), and solubility product (K_{sp}) values in water, alongside the crystal structures usually encountered in SNCs.

Because of these properties, in the literature there are several examples of applications of Ag₂E SNCs for imaging and sensing in the biomedical context. For example, Pang et al. have proposed sub-3 nm Ag₂Se SNCs whose NIR emission can be finely tuned by controlling the ratio between Ag and Se. The optimized 820 nm-emitting (NIR-I) Ag₂Se SNCs enabled deep-tissue imaging in living nude mice [30]. Yet, NIR-II emission generated upon NIR-I excitation has been shown to be so far the most favourable combination for *in vivo* applications, given the high tissue penetration and spatial resolution achievable [31,32]. To that end, NIR-II emitting Ag₂S SNCs have been used as nanothermometers to

Table 1
Properties of Ag₂E materials [26,27].

Material	E_g , eV	r_B , nm	K_{sp}	Crystal phases
Ag ₂ S	0.9–1.1	2.2	$6 \cdot 10^{-50}$	Monoclinic ^b (α , acanthite, $P2_1/c$), cubic body-centred (β , argentite, $Im-3m$), cubic face-centred (γ , $Fm-3m$)
Ag ₂ Se	0.15	2.9 [28]	$2 \cdot 10^{-64}$	Orthorhombic ^b (β , $P2_12_12_1$), cubic (α , $Im-3m$)
Ag ₂ Te	0.67 (β), 0.025 (α) [29]	N/A ^a	$2 \cdot 10^{-72}$	Monoclinic ^b (α , $P2_1/c$), cubic body-centred (β , $Im-3m$), cubic face-centred (γ , $Fm-3m$)

^a Not yet clearly defined.

^b Low-temperature stable phases.

realize remote, real-time brain temperature monitoring [10], as well as *in vivo* thermal monitoring during magnetic hyperthermia treatments with high thermal resolution (0.2 °C) [11]. Along the same lines, 1300 nm-emitting Ag₂Te SNCs have been used for tumour imaging by Zhang et al. [33]. The authors modified the SNCs with poly(lactic-co-glycolic acid) (PLGA) and encapsulated them using 4T1 cell membrane, which ensured selective targeting of breast cancer cells. These are just but a few of the publications on the use of NIR-operating Ag₂E SNCs for *in vivo* imaging and biosensing, which showcase the great potential of this family of nanomaterials.

While the prowess of Ag₂E SNCs in the biomedical context is undeniable, the performance of these nanomaterials is generally affected by a poor PLQY (often below 1%). This magnitude contributes to define the key feature of a luminescent contrast agent or nanosensor: the brightness (the product between the molar absorption coefficient (ϵ) and the PLQY). Indeed, a higher brightness directly translates to a higher signal-to-noise ratio, and hence a higher spatial and temporal resolution, as well as a higher precision of the luminescence sensing approach [15,34]. Although Ag₂E SNCs can count on a large ϵ (e.g., for Ag₂S SNCs this value is approximately $4\text{--}5 \cdot 10^5 \text{ M}^{-1} \text{ cm}^{-1}$ at 800 nm [35]), their poor PLQY represents a strongly limiting factor. The low value of PLQY in Ag₂E SNCs should be retraced to the low solubility product of the material (for syntheses in aqueous media) and the high mobility of Ag⁺ ions in the lattice. These factors lead, respectively, *i)* to the difficulty to

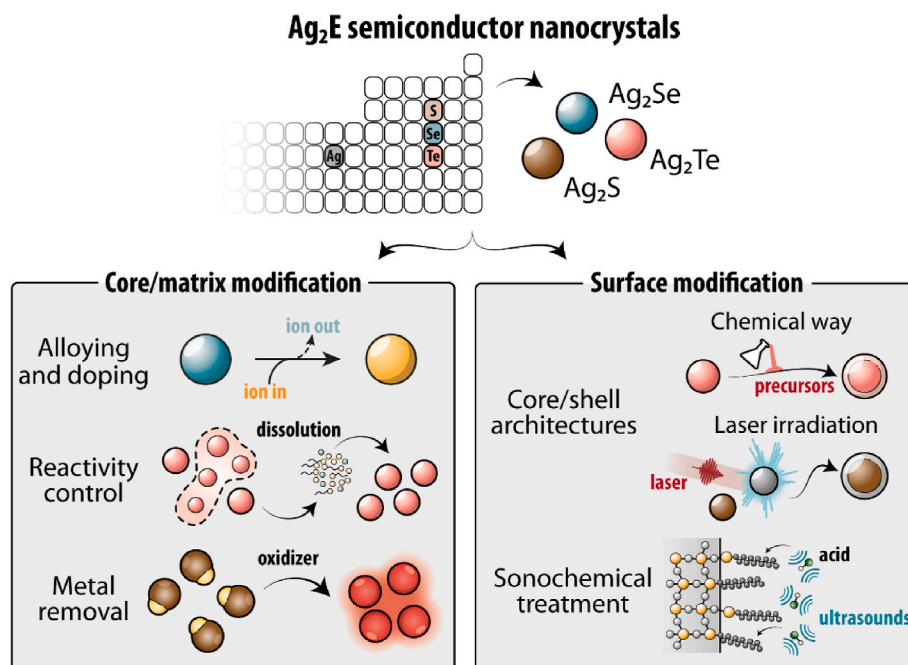


Fig. 1. Overview of the methods for increasing the PLQY of Ag₂E SNCs.

control the rate of formation of the SNCs during the synthesis and *ii*) the presence of cation vacancies/crystal defects in the core and the surface that act as luminescence quenching centers [15,36–38]. Additionally, like any nanoparticle, SNCs have high surface-to-volume ratios. This feature exacerbates the issue of surface quenching: a process whereby surface trap states and interaction with high-energy ligand or solvent molecules leads to the non-radiative depopulation of excited states. Several approaches have therefore been developed to tackle the limitation of low PLQY in the otherwise promising family of Ag₂E SNCs. These approaches can be divided in two families:

1) *Methods for optimization of the core material:*

- control of the chemical reactivity of the synthesis mixture (Section 3.1);
- alloying and doping (Section 3.2);
- selective oxidation (Section 3.3).

2) *Methods for optimization of the surface:*

- post-synthesis sonochemical treatment (Section 3.4);
- growth of core/shell architectures (Section 3.5);
- ultrafast laser irradiation (Section 3.6).

Below, we provide a general description of each approach – when relevant –, later detailing how it has been applied specifically to Ag₂E SNCs.

3. Methods to improve the PLQY in Ag₂E SNCs

3.1. Chemical control

Ag₂E SNCs can be synthesized, both in aqueous and in organic media, using relatively fast and straightforward synthetic methods. The most widely used procedure to obtain monodispersed Ag₂E SNCs with controlled size is the thermal decomposition of single source precursors in organic media [20,39]. Yet, even if the methodology seems simple, obtaining SNCs with high PLQY is challenging due to two main reasons:

1. The **high redox potential** of Ag⁺ ions in the presence of possible reducing agents – like dodecylamine [40] – acting as capping agent and the use of high reaction temperatures. Because of this, an Ag-enriched core is often formed – which can act as quenching moiety (see Section 3.3) – reducing the number of Ag⁺ ions available to form the semiconductor (Ag₂E). Other molecules that are used in the synthesis of Ag₂E SNCs as solvent and capping agent – like 1-dodecanethiol (DDT) – can also act as mild reducing agents [41].
2. The **high mobility** of the Ag⁺ ions inside the Ag₂E matrix creates defects in the crystalline structure. These introduce in-gap states that favor non-radiative relaxations, thus reducing the photoluminescence efficiency of the SNCs. For example, the α -Ag₂S (acanthite phase) monoclinic structure is composed of two structural sublattices, a rigid immobile sublattice of S²⁻ anions and a mobile migrant sublattice of Ag⁺ cations [37]. Deviations from stoichiometry are often encountered in inorganic substances and even more so at the nanoscale (where surface effects and lattice distortions are dominant), given that this effect is highly dependent on the size of the crystals. To that end, bulk α -Ag₂S is a stoichiometric compound. However, below 50 nm, vacancies in the metal sublattice have been often observed, yielding non-stoichiometric structures with a considerable impact on the properties of Ag₂S SNCs [42].

Given the above, the first step towards bright Ag₂E SNCs is to chemically control the formation of the crystal structure, thus minimizing non-radiative matrix defects. To that end, Ortega-Rodríguez et al. systematically studied how changing in the reaction mixture the molar fraction of DDT and oleylamine (OAm) – acting simultaneously as solvent and capping agent – allows achieving a fine control over the properties of Ag₂S SNCs prepared from the thermal decomposition of

silver diethyldithiocarbamate (Ag-ddtc; Fig. 2a and b) [43].

Specifically, it was shown that the synthetic conditions greatly affected the size, the position of the Ag-enriched core within the SNC, and the stoichiometry of the Ag₂S structure. The SNCs with highest PLQY (approximately 2%) were obtained using a DDT mole fraction $\chi_{\text{DDT}} = 0.6$ in the solvent (DDT + OAm) mixture. This result was explained considering the different roles played by the two molecules. OAm lowers the dissociation energy of the C–S bonds of the silver-sulfur organic precursor to release a higher amount of reactive sulfur available for the Ag₂S formation [44]. On the other side, the high binding energy of the DDT towards silver was exploited to stabilize the formed Ag₂S [45]. Upon finding the “sweet spot” in terms of reaction mixture composition, SNCs with a refined Ag₂S matrix were obtained, showing a homogeneous distribution of silver and sulfur and a Ag/S ratio close to the stoichiometric one (Ag/S = 2), ultimately yielding a 10-fold increase in the PLQY compared to SNCs prepared only in presence of OAm.

Moving our attention to a different chalcogenide, already in 2011 Yarema et al. synthesized Ag₂Te SNCs with NIR emission and a PLQY of 1.7% [46]. Later, this value was improved by Zhang et al., who obtained Ag₂Te SNCs with tuneable emission (emission peak centre from 950 to 2100 nm) and absolute PLQY reaching up to 12% by regulating the reactivity of the silver precursors using tertiary phosphine [47]. Organic silver thiolates were prepared as silver precursors, which were subsequently reacted with a Te-tributylphosphine (Te-TBP) solution at high temperature [48]. The authors imputed the large tunability range and narrowness of the emission spectra of the prepared Ag₂Te SNCs (and hence their monodispersity in size) to the phosphine-supported increased reactivity of the silver precursors and to a size-focusing effect, whereby some of the smaller crystals are redissolved to provide further precursors for the controlled growth of the SNCs (Fig. 2c). The effect of the tertiary phosphine on the resulting SNCs was later further investigated comparing the Ag₂Te SNCs prepared in the presence of alkyl phosphines (e.g., trioctylphosphine (TOP)) and aryl phosphines (e.g., triphenylphosphine (TPP)) [48]. It was shown that the stronger affinity of TOP towards Ag⁺ resulted in the displacement of the thiolate molecules, yielding a silver precursor with higher reactivity (Fig. 2d). On the other hand, TPP forms weaker Ag–P bonds, leaving Ag–S bonds that effectively reduce the reactivity of the silver precursor. The weaker interaction of the TPP with Ag⁺ widens the concentration range of phosphine that can be introduced in the reaction mixture before the reactivity is increased uncontrollably. As a result, the growth of SNCs with a less defective crystal structure is enabled and hence higher PLQY (up to 14.7%).

3.2. Alloying and doping strategies

Alloying with iso- or aliovalent metal ions is one of the most efficient and straightforward strategies to enhance the PLQY of different SNCs. This approach has been demonstrated, among others, for ZnSe [49–51], CdS [52–54] and, of course, Ag-based SNCs [55,56].

Regarding this last family of materials, in 2016 Song et al. obtained ternary AgInS₂ SNCs ($\lambda_{\text{em}} = 670$ nm) via cation exchange (CE) starting from Ag₂S SNCs. The PLQY of the AgInS₂ SNCs reached 32%, and the optical properties could be tuned by modulating the In³⁺/Ag⁺ ratio [57]. In 2020, Shu et al. reported that Pb-doped Ag₂S SNCs, prepared by introducing (Pb(NO₃)₃)₂ in the reaction mixture, showed improved emission intensity with a PLQY up to 4% and tuneable emission wavelength from 950 to 1200 nm [58]. A similar strategy was employed by Wang et al. to improve the PLQY of Ag₂Se SNCs alloying them with Au, thus obtaining AgAuSe SNCs (Fig. 3a–c). Also in this case, doping with different Au³⁺ amounts resulted in tuneable emission wavelength, with higher concentration of gold yielding a more pronounced blue-shift [36]. The claimed PLQY for the brightest sample was 65.3% with an emission maximum centred at 978 nm. This high PLQY was attributed to the decrease in non-radiative transition of excitons thanks to the suppression of cation vacancies and crystal defects induced by the

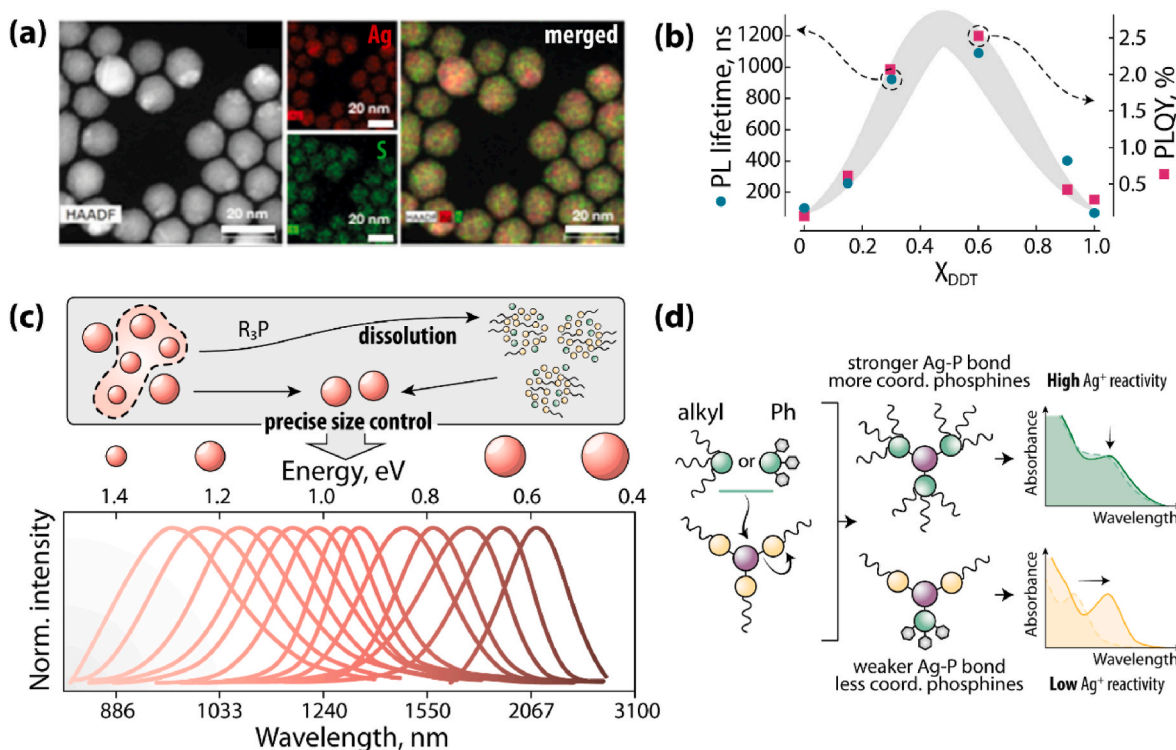


Fig. 2. Control of the precursor reactivity. (a) High-angle annular dark-field scanning transmission electron microscopy (HAADF STEM) micrograph and corresponding Energy-Dispersive X-ray Spectroscopy (EDS) elemental maps of Ag₂S SNCs obtained using a 1-dodecanethiol (DDT) mole fraction of 60% (in the reaction mixture of DDT and oleylamine). (b) Trend of PLQY and photoluminescence (PL) lifetime as a function of DDT mole fraction in the reaction mixture. Adapted with permission from *ACS Appl. Mater. Interfaces* **2020**, *12*, 12500–12509. (c) Scheme of the effect of tertiary phosphines in the reaction mixture during the synthesis of Ag₂Te SNCs along with the wide emission range that can be spanned controlling the growth of these nanomaterials. Adapted with permission from *J. Am. Chem. Soc.* **2021**, *143*, 12867–12877. (d) Scheme of the difference in reactivity control that can be achieved using alkyl or aryl phosphines during the growth of Ag₂Te SNCs. Adapted with permission from *Chem. Mater.* **2021**, *33*, 9524–9533.

incorporation of Au in the matrix. The same group later proposed the doping of Ag₂Se SNCs with Pb²⁺ via CE (Fig. 3d–f) [59].

The resulting Ag₂Se:Pb²⁺ SNCs featured NIR-II emissions that were 4 times more intense than before exchange. After proper surface functionalization with polyethylene glycol (PEG), these SNCs were used to monitor the lymphatic drainage system via high-resolution NIR-II imaging. The approach was also reported for Ag₂Te SNCs, which were doped with Au again following a CE protocol [60]. The SNCs doped with 4% of Au showed an emission centred at 1600 nm and a 12-fold increase in PLQY compared to parent Ag₂Te SNCs. Also in this case, the authors postulated a reduction of defects that brings about a suppression of quenching pathways, supporting their claim with an overall lengthening of the photoluminescence lifetime in doped SNCs.

3.3. Selective oxidation

We already highlighted in Section 3.1 how metallic silver nanoparticles can be present in the Ag₂E SNCs dispersion as by-products of the synthesis. This comes as no surprise, given the high reduction potential of Ag⁺ (0.7996 V). This aspect of the silver chemistry plays a central role in Ag₂E SNCs. Indeed, during the synthesis Ag⁰ nanoparticles can be formed rapidly, and they act as heterogeneous nuclei upon which the Ag₂E SNCs grow. The resulting structure is a dimeric/Janus nanomaterial featuring a metallic and a semiconducting moiety in physical contact. This configuration facilitates the exchange of electrons between the two moieties, effectively subtracting excited electrons from the semiconductor and introducing non-radiative electron de-excitation pathways [61]. Selective removal of the metallic part can therefore help reducing processes responsible for luminescence quenching.

Indeed, in 2021, Song et al. showcased how Ag/Ag₂S Janus

nanoparticles exhibited quenched emission due to electron transfer between Ag and Ag₂S [62]. The emission intensity of the nanomaterial was enhanced after the selective oxidation of Ag⁰ in the presence of H₂O₂. Broadly speaking, oxidation-induced emission enhancement in nanoparticles is a strategy employed to achieve smart responsive diagnosis, since H₂O₂ is overexpressed in tumour microenvironment (TME) [63–66]. Therefore, the H₂O₂-mediated etching of Ag endows the Ag/Ag₂S Janus nanoparticles with TME-responsive NIR-II (1250 nm) emission capabilities (Fig. 4a–c).

Marin et al. used a similar concept to transform Ag/Ag₂S dimers into Ag₂S SNCs, hence turning them from photoacoustic (PA) to fluorescence imaging contrast agents [67]. These nanoparticles were synthesized via a green synthesis method entailing the use of store-bought roasted coffee extracts as the source of ligands controlling the particle growth. The complete lack of photoluminescence of the as-synthesized Ag/Ag₂S dimers make them ideal PA contrast agents, since they are capable of effectively transducing the absorbed optical energy into heat, hence locally generating acoustic waves (the signal used in PA imaging). Upon exposing the Ag/Ag₂S dimers to H₂O₂, their photoluminescence was switched on, thanks to the selective removal of the metallic, plasmonic moiety, hence obtaining Ag₂S SNCs. The suitability of the Ag/Ag₂S dimers and Ag₂S SNCs as PA and fluorescence imaging contrast agents, respectively, was then demonstrated at the *in vivo* level (Fig. 4d–e).

This strategy thus not only afford Ag₂E SNCs with higher PLQY values, but also smart nanoprobe with on/off luminescence that can be activated in the presence of oxidizing environments, such as H₂O₂-rich TMEs.

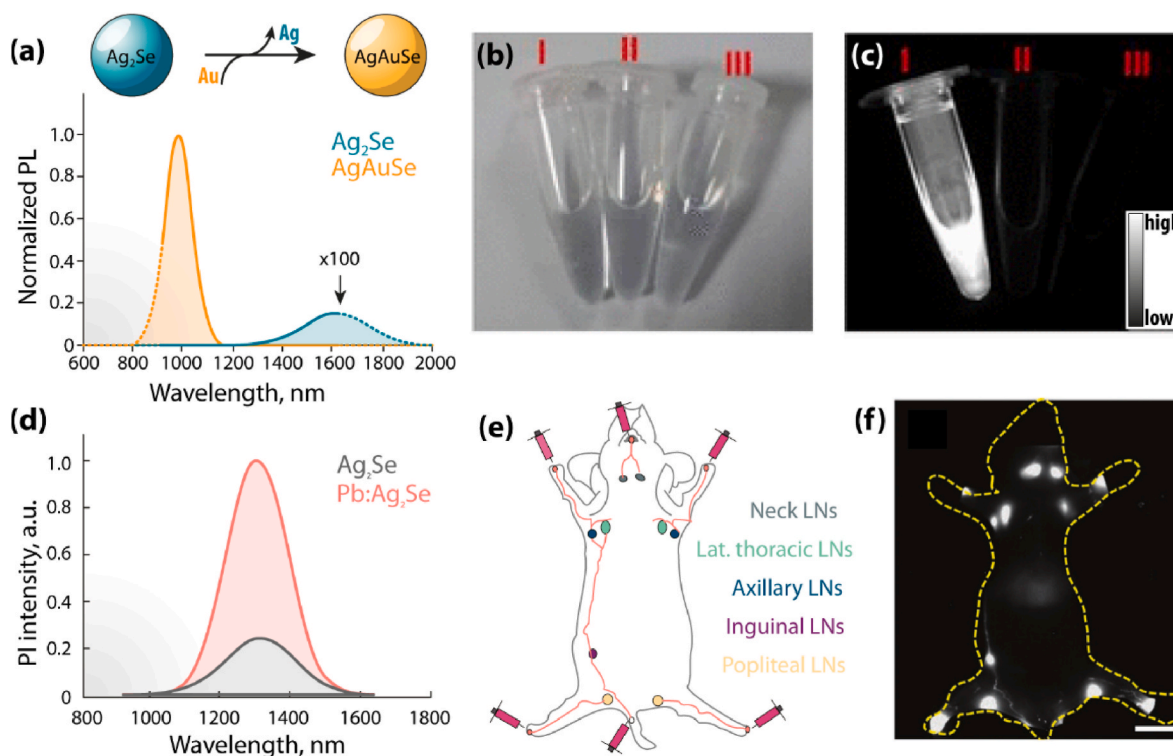


Fig. 3. Alloying and doping strategies in Ag_2E SNCs. (a) Cation exchange from Ag_2Se to AgAuSe and their photoluminescence (PL) emission spectra. (b) Optical images and (c) corresponding NIR images of colloidal dispersions of AgAuSe and Ag_2S SNCs in cyclohexane (I, 1060 nm AgAuSe SNCs; II, 1050 nm Ag_2S SNCs; III, pure cyclohexane). Adapted with permission from *J. Am. Chem. Soc.*, **2021**, *143*, 2601–2607. (d) Room-temperature PL spectra of 3.8-nm-diameter Ag_2Se and $\text{Ag}_2\text{Se}:\text{Pb}^{2+}$ SNCs dispersed in tetrachloromethane ($\lambda_{\text{ex}} = 785$ nm). (e) Schematic illustration of major lymphatic system and injecting sites of supine whole-body nude mouse. (f) NIR-II imaging for major lymph nodes (LNs). Adapted with permission from *Small* **2021**, *17*, e2006111.

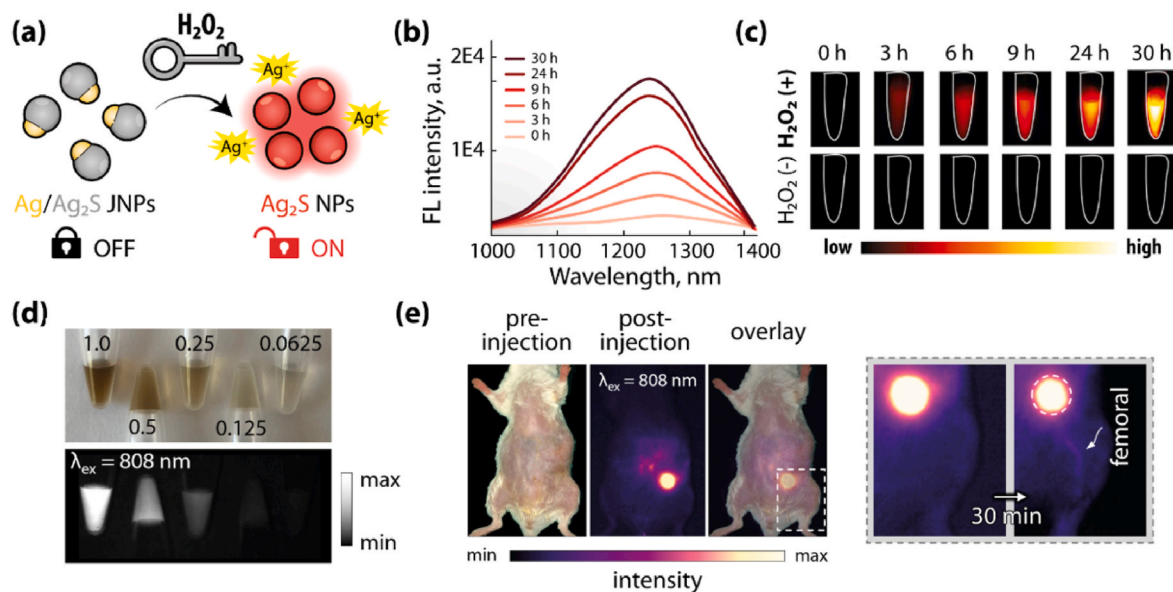


Fig. 4. Selective oxidation of the metallic core. (a) Schematic illustration of the mechanism of activation of $\text{Ag}/\text{Ag}_2\text{S}$ Janus nanoparticles (JNPs) with H_2O_2 -activated NIR-II fluorescence. (b) Fluorescence spectra of $\text{Ag}/\text{Ag}_2\text{S}$ JNPs treated with H_2O_2 at different times. (c) NIR-II fluorescence images of $\text{Ag}/\text{Ag}_2\text{S}$ JNPs at 1250 nm in an aqueous dispersion at different times after treatment with/without H_2O_2 . Adapted with permission from *Nano Lett.*, **2021**, *21*, 2625–2633. (d) Optical (top) and NIR (bottom) images of 1.5-mL centrifuge tubes filled with different concentrations (1, 0.5, 0.25, 0.125, 0.0625 mg mL^{-1}) of Ag_2S SNCs dispersions obtained via coffee-mediated synthesis and after treatment with H_2O_2 . (e) In vivo NIR photoluminescence images obtained after intraperitoneal injection of 50 μL of a 1 mg mL^{-1} dispersion of the same Ag_2S SNCs. Adapted with permission from *Adv. Photonics Res.*, **2021**, *3*, 2100260.

3.4. Sonochemical treatment

SNCs have large values of surface-to-volume ratio (SVR),

consequently, passivation of surface defects is required to produce high-quality nanocrystals [68]. This is where organic molecules come into play as ligands that interact with the metallic ions exposed on the SNC

surface to reduce dangling bonds. Thus, understanding the organo-metallic interactions that take place on the SNC surface is of great significance to reduce non-radiative surface trap states [69]. In the case of Ag_2E SNCs, thiol-terminated organic molecules are frequently used as solvents and capping agents [70,71], because thiol groups exhibit the highest binding energy towards silver atoms (216 kJ/mol) [72–74]. Nevertheless, thiol-terminated capping agents, such as DDT, could act as hole traps, reducing the PLQY of the SNCs.

Surface etching has been an extensively used strategy to reduce surface defects enhancing the efficiency of the treated NPs. For instance, HF has been employed to increase the PLQY of InP SNCs since 1996 [75], achieving the removal of surface molecules that could generate non-radiative recombination pathways [76–79]. However, the direct addition and handling of corrosive molecules like HF make this approach hazardous. An alternative to this method was developed by Zabala-Gutierrez et al. [13], who tackled the matter of controllably etching the surface of Ag_2E SNCs in an indirect way. More specifically, the authors developed a post-synthetic treatment to increase the PLQY of Ag_2S SNCs from 2 to 10% via ultrasonication in chloroform (Fig. 5). The surface of as-synthesized SNCs is covered by an excess of DDT molecules bound to the Ag^+ ions. The post-synthetic treatment generates a small quantity of HCl following the decomposition of chloroform. The HCl generated *in situ* induced a sonochemical-assisted etching of the SNC surface, as evidenced by a slight reduction of the Ag_2S SNC size. Moreover, some of the more loosely bound DDT molecules were removed from the SNC surface. DDT features a high electron density stemming from the two lone pairs of the surface-bound thiol groups, which can act as fast hole traps, ultimately reducing the PLQY of the SNCs by quenching [80–82].

Therefore, the reduction in the number of *surface-bound* DDT molecules that followed the sonochemical etching process led to SNCs mostly stabilized through *crystal-bound* DDT molecules – whose presence has been reported in nanoparticles prepared at high temperatures using DDT as a solvent [83]. This latter type of DDT molecules does not contribute as heavily to quenching, since they have their thiol groups embedded within the Ag_2S crystal matrix. The embedment of these thiols in the crystal structure of Ag_2S SNCs was also confirmed by an increase in the Ag/S ratio closer to 2 (the theoretical stoichiometry of Ag_2S) after sonochemical treatment.

3.5. Core/shell structures

The preparation of core/shell architectures is a well-known strategy to increase the PLQY of SNCs and finely modulate their optical properties, with its first reports dating back to the beginning of the 90's [84,

85]. There are several excellent reviews about core/shell SNCs [86–88], and the landscape of core/shell SNCs is almost limitless, with countless variations in terms of core and shell composition, thickness, and complexity of the structure.

One of the most widely employed strategies when a higher PLQY is sought after is the growth of a shell of a semiconductor material with a wider bandgap than the one of the core material. This is the case for the iconic CdSe/ZnS SNCs [86,89], where the energy gap of the core and shell are 1.7 and 3.6 eV, respectively. This type of structure is referred to as Type I core/shell, wherein the shell increases the optical performance of the SNCs because:

- upon its growth, dangling bonds at the core surface (which act as localized defects responsible for quenching) are removed;
- it increases the distance between the core and molecules with high-energy vibrations (such as water) that contribute to non-radiative relaxation events;
- the shell acts as an energy barrier, effectively confining the exciton wavefunction within the core volume.

The growth of a ZnS shell has been reported in a handful of instances for Ag_2S SNCs [18,90,91]. All those reports deal with Ag_2S of small size with emission in the red/NIR-I, and generally with dismal initial values of PLQY. Chen et al. developed instead $\text{Ag}_2\text{Te}/\text{ZnS}$ SNCs whose emission falls in the NIR-II [92]. The synthesis of these SNCs entails the preparation of sacrificial CdTe SNCs, which are transformed into Ag_2Te via CE followed by the growth of a ZnS shell. PLQY of 5.6% and an emission peak centred around 1100 nm characterized the core/shell SNCs. Astonishingly, all the steps of the synthesis were conducted in water and, hence, at relatively low temperature. The PLQY values obtained in Ag_2E with a shell of ZnS, however, are by no means comparable with the ones obtained with other core SNCs such as the previously mentioned CdSe and CuInS_2 [93], for example. Aside from the poor initial PLQY of the Ag_2E core, the large lattice mismatch (16%) between ZnS and Ag_2E is a major limiting factor for growing high-quality core/shell SNCs using ZnS as the shell material. Indeed, matchstick-like heterostructures have been obtained in some instances when growing ZnS on Ag_2S SNCs cores [94, 95].

A way around this impasse was found, for example, by Zhang et al., who grew core/shell SNCs of $\text{Ag}_2\text{Te}/\text{Ag}_2\text{S}$ (Fig. 6) [96]. The growth of a shell of Ag_2E with a larger bandgap than the Ag_2E making up the core allowed increasing the emission efficiency by 3.2 times, with a final PLQY of 4.3% and an emission centred at 1300 nm. A similar core/shell SNC was also prepared with a larger Ag_2Te core, which allowed pushing the emission of the final $\text{Ag}_2\text{Te}/\text{Ag}_2\text{S}$ above 1500 nm, in NIR-III.

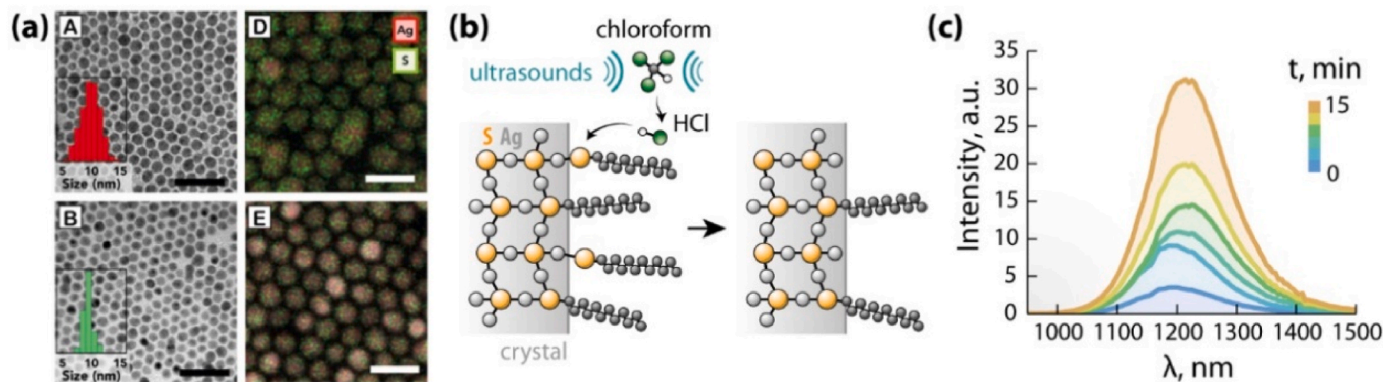


Fig. 5. Sonochemical treatment for surface restructuring of Ag_2S SNCs. (a) TEM micrographs (left) of Ag_2S SNCs before (top) and 9 min into ultrasonication treatment (bottom), along with the corresponding EDS elemental maps showing Ag in red and S in green. Scales bars are 50 nm for the TEM micrographs and 20 nm for EDS elemental maps. The insets within the TEM micrographs depict the size distribution of the SNCs, showing a slight reduction in size after ultrasound treatment in chloroform. (b) Scheme of the proposed mechanism of surface modification induced via ultrasound treatment of a dispersion of Ag_2S SNCs in chloroform. (c) Trend of the emission intensity as a function of sonication time. Adapted with permission from ACS Appl. Mater. Interfaces 2022, 14, 4871–4881.

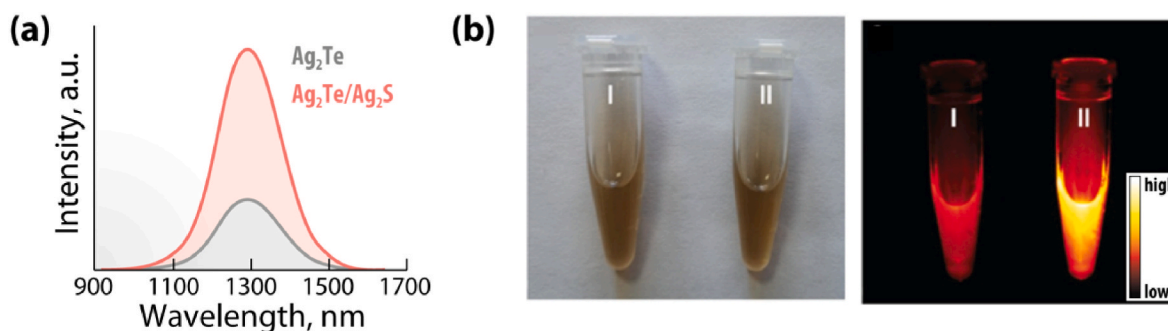


Fig. 6. Core/shell architectures. (a) The emission efficiency of Ag_2Te SNCs can be increased by growing a shell of Ag_2S . (b) The NIR-II emission intensity under NIR-I excitation is higher for the core/shell SNCs. I: core, II: core/shell. Adapted with permission from *Small* 2020, 16, 2001003.

3.6. Ultrafast laser irradiation

As it is explained further below, this approach has been shown to ultimately yield core/shell structures in the case of Ag_2S SNCs, and the reason for the PLQY enhancement can be traced back to the explanations provided in Section 3.5. However, we decided to discuss this approach separately, given the unique way in which the growth of the shell is achieved compared to more commonly employed chemical methods.

Ultrafast lasers can generate super short (in the femtosecond range), and hence highly energetic pulses (over 1 mJ per pulse) [97]. Ultrafast laser irradiation has been widely used in several areas [98–100], including chemical or physical analysis [97], material processing [101, 102], and the medical field [103,104]. In 1987, Srinivasan was the first to report on the femtosecond ultraviolet excimer laser for controlled polymethyl methacrylate etching [105], followed by Kuper et al. [106]: A method that allows achieving ultra-high precision manufacturing of materials. Since then, ultrafast lasers have been adopted as a powerful tool for material processing [107,108]. Focusing on nanomaterials, Zhu et al. obtained atomic restructuring of monocrystalline Au nanoparticles via ultrafast laser irradiation to improve their surface activity, testing the performance of the nanoparticles in the model reaction of 4-nitrophenol reduction [109]. Ultrafast laser has also been applied for the preparation of nanomaterials in solution via laser ablation. To that end,

Nguyen et al. prepared boron nitride quantum dots with tuneable photoluminescence (from UV to green) by laser ablation of boron nitride powder suspended in different media (ethanol, diethylamine, and ethylenediamine) [110].

Following in these footsteps, in a previous work Santos et al. induced an 80-fold PLQY enhancement in Ag_2S SNCs through femtosecond laser irradiation (Fig. 7). This enhancement was generated thanks to the growth of a protective AgCl shell on the SNC surface [35]. More specifically, the process entails a laser-induced Coulomb explosion of Ag^0 nanoparticles that can absorb the excitation photons due to the presence of virtual energy states. These metallic nanoparticles are present alongside Ag_2S SNCs in the chloroform (CHCl_3) dispersion because they are formed as side product during the colloidal synthesis.

The formation of Ag^+ proceeding from the Coulomb explosion is followed by its reaction with Cl^- generated *in situ* by the decomposition of CHCl_3 molecules. The AgCl that is thusly formed is then deposited as a shell on the Ag_2S SNCs reducing the number of surface traps and minimizing the solvent-mediated non-radiative relaxation events.

4. Conclusions and perspectives

From the above discussion, it is apparent that the application of Ag_2E SNCs in the field of bioimaging and sensing has been accompanied by a

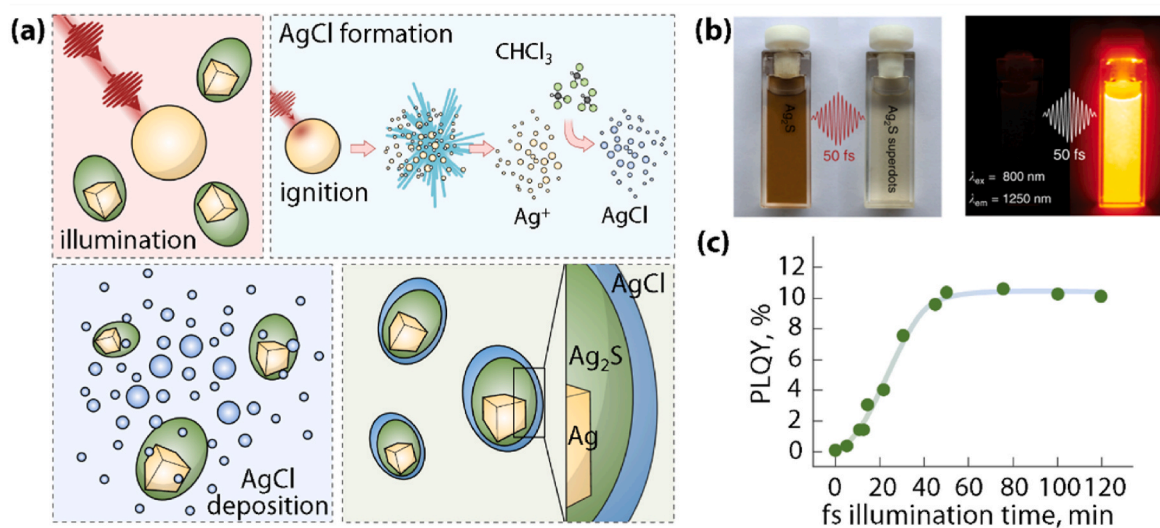


Fig. 7. Surface modification via ultrafast laser irradiation. (a) Schematic representation of the physicochemical mechanisms underlying the ultrafast laser-induced transformation. Upon illumination with ultrafast infrared laser pulses, multiphoton excitation of Ag^0 nanoparticles leads to their Coulomb explosion. The silver ions generated in this process react with CHCl_3 molecules forming AgCl , which in turn reacts with the surface of the Ag_2S SNCs forming a protective layer. (b) Optical image and NIR-II fluorescence image of a colloidal dispersion of Ag_2S SNCs in CHCl_3 before (left) and after (right) ultrafast laser irradiation (50 fs, 90 min, 9 W cm^{-2}). (c) PLQY of the Ag_2S SNCs after being subjected to ultrafast laser irradiation processes of different durations. Adapted with permission from *Nat. Commun.* 2020, 11, 2933.

steady effort to improve the optical properties of this family of nanomaterials. Specifically, a little over ten years' worth of investigation bore several fruits in terms of strategies to modify either the core or the surface of these SNCs to increase their PLQY. Simultaneously, a deeper understanding of the chemical and physical behaviour of Ag₂E SNCs has been achieved, granting access to strategies to better tune their optical properties. A comparison of the performance of each strategy is provided in Table 2.

Of course, this research has been supported by decades of experience in the preparation of SNCs like quantum dots of CdSe and PbS, and the strategies developed for those materials were adapted to the needs of Ag₂E SNCs.

From the survey of the literature that we performed, control of the reactivity of the precursor mixture emerges as the essential initial step towards high-quality Ag₂E SNCs. Variations in the nature of the ligands, their relative content, reaction time and temperature, along with the

type of metal precursor employed all contribute to determining the quality of the SNCs through tuning of the size, crystal lattice integrity, stoichiometry, and homogeneous distribution of the elements throughout the SNC volume. Given the extended library of ligands available nowadays, it is not unlikely that other molecules – and combinations thereof – will be identified in the future that can grant an even finer control over the properties of Ag₂E SNCs.

Alloying presents itself as a powerful approach to enhance and modulate the optical properties of Ag₂E SNCs. However, to rationally improve different kinds of Ag₂E via alloying and/or doping, it is necessary to fully understand the enhancement mechanism and how different types of metals can alter band-edge electronic states and/or introduce impurity-bound states. Theoretical modelling and low temperature optical characterization (e.g., time-resolved and transient absorption spectroscopy) can act synergistically in this sense, unveiling the mechanisms underpinning the spectroscopy of Ag₂E SNCs. Studies in single particles can also help identifying the interparticle variability within the same SNC batch.

While not all the Ag₂E SNCs reported in the literature display an Ag-rich core, selective oxidation of the metal moiety is an easily implementable strategy for turning on or increase the PLQY. Although this approach has been demonstrated using H₂O₂ as the oxidizer, possibly other oxidizing agents can be employed, like elemental oxygen (O₂) bubbled in the Ag₂E SNC dispersion.

Turning the attention to strategies to modify the SNC surface, a purely chemical approach for the growth of core/shell structure has yielded limited PLQY enhancement – albeit it being the standard approach for other SNCs. Irradiation with femtosecond laser – a physical technique – has so far proven the most effective strategy to grow a passivating shell. But it has been demonstrated only for Ag₂S SNCs and when elemental Ag nanoparticles are present in dispersion. This approach might be viable also for other Ag₂E SNCs and, possibly, it can be made more versatile via the intentional addition of controlled amounts of metallic nanoparticles in the irradiated dispersion. Yet, ultrafast lasers are not readily available, which makes the spreading of this strategy on a large scale unlikely. On the other hand, a tip sonicator is a common piece of equipment in most chemistry laboratories. Therefore, the controlled sonochemical treatment developed for Ag₂S SNCs is more easily accessible, and it would be intriguing to explore the effect that such treatment has on other Ag₂E SNCs.

The values of PLQY achieved implementing some of these strategies – in hand with the high light absorption efficiency typical of semiconductors – make these nanomaterials bright enough to represent the staple NIR emitting SNCs lacking heavier elements like Pb and Hg. Nonetheless, we expect that the performance of Ag₂E-based SNCs could be further improved by combining two or more of the above approaches. The group of Prof. Rubio-Retama already moved along these lines optimizing first the precursors reactivity to prepare Ag₂S SNCs and subsequently applying sonochemical treatments. The PLQY could possibly be further increased by a controlled oxidation of the Ag-rich core and/or the growth of a shell via chemical means. Alternatively, the sonochemical treatment can be applied after a cation exchange has been performed to introduce metal ions. The combinations are virtually limitless, and it is not to be discounted that artificial intelligence could lend a hand in this sense, identifying the most promising combination of approaches to achieve near-unity PLQY in a Ag₂E-based SNC.

To conclude, Ag₂E SNCs are a versatile family of nanomaterials with quite literally a bright future particularly in the field of nanotechnology-supported biomedicine. We hope that this article will spur even further investigation on these nanomaterials, towards untapping their full potential.

Declaration of competing interest

The authors declare the following financial interests/personal relationships which may be considered as potential competing interests:

Table 2
Comparison of different strategies for improving the PLQY of Ag₂E SNCs.

Method	Advantages	Disadvantages	PLQY improvement (n-fold)
<i>Chemical control</i>	<ul style="list-style-type: none"> • Easy to implement • Applicable to different Ag₂E SNCs • Enables tuning of the emission wavelength • Large variety of molecules available 	<ul style="list-style-type: none"> • Relatively low final PLQY 	0.2% → 2.3% (10) [43], 2% → 12% (6) [47], 2.1% → 14.7% (7) [48]
<i>Alloying and doping</i>	<ul style="list-style-type: none"> • Easy to implement • Applicable to different Ag₂E SNCs • Enables tuning of the emission wavelength • Several elements available for testing 	<ul style="list-style-type: none"> • Lack of clear understanding of the enhancement origin 	9.6% → 65.3% (7) [36], 6% → 32% (5) [57]
<i>Selective oxidation</i>	<ul style="list-style-type: none"> • Easy to implement • Smart on-off probes can be obtained • Slow oxidation allows fine control to be achieved 	<ul style="list-style-type: none"> • Limited selective oxidation reagents 	Activation from no luminescence [62,67]
<i>Sonochemical treatment</i>	<ul style="list-style-type: none"> • Easy to implement • Highly controllable 	<ul style="list-style-type: none"> • Demonstrated only for Ag₂S • Requires tip sonicator • Relatively low final PLQY 	2% → 10% (5) [13]
<i>Core/shell structures</i>	<ul style="list-style-type: none"> • Applicable to different SNCs 	<ul style="list-style-type: none"> • Poor PLQY enhancement or observed starting from low values • Reduced available materials for shell 	0.02% → 3.8% (190) [18] - (4.5) [85], 0.15% → 2.91% (18) [86], 1.3% → 4.3% (3.2) [91]
<i>Ultrafast laser irradiation</i>	<ul style="list-style-type: none"> • Highest achievable enhancement 	<ul style="list-style-type: none"> • Demonstrated only for Ag₂S • Relies on the presence of Ag(0) synthesis byproducts • Requires ultra-fast laser 	0.13% → 10.7% (82) [35]

Riccardo Marin reports financial support was provided by Spain Ministry of Science and Innovation. Irene Zabala-Gutierrez reports financial support was provided by UCM-Santander. Liyan Ming reports financial support was provided by China Scholarship Council.

Data availability

No data was used for the research described in the article.

Acknowledgements

This work was financed by the Spanish Ministerio de Ciencia e Innovación under project NANONERV PID2019-106211RB-I00, NANOGRANZ PID2021-123318OB-I00, PID2021-122806OB-I00 and TED2021-132317-I00B, by the Instituto de Salud Carlos III (PI19/00565), by the Comunidad Autónoma de Madrid (P2022/BMD-7403 RENIM-CM) and co-financed by the European structural and investment fund. R.M. is grateful to the Spanish Ministerio de Ciencia e Innovación for support to research through a Ramón y Cajal Fellowship (RYC2021-032913-I). I.Z.-G. thanks UCM-Santander for a predoctoral contract (CT63/19-CT64/19). L.M. acknowledges a scholarship from the China Scholarship Council (No. 202108350018).

References

- [1] R.G. Aswathy, Y. Yoshida, T. Maekawa, D.S. Kumar, Near-infrared quantum dots for deep tissue imaging, *Anal. Bioanal. Chem.* 397 (2010) 1417–1435.
- [2] S. Xu, J. Cui, L. Wang, Recent developments of low-toxicity NIR II quantum dots for sensing and bioimaging, *TrAC, Trends Anal. Chem.* 80 (2016) 149–155.
- [3] P. Zhao, Q. Xu, J. Tao, Z. Jin, Y. Pan, C. Yu, Z. Yu, Near infrared quantum dots in biomedical applications: current status and future perspective, *WIREs Nanomed. Nanobi.* 10 (2018) e1483.
- [4] C. Ding, Y. Huang, Z. Shen, X. Chen, Synthesis and bioapplications of Ag(2)S quantum dots with near-infrared fluorescence, *Adv. Mater.* 33 (2021), e2007768.
- [5] M. Jiao, A.S. Portniagin, X. Luo, L. Jing, B. Han, A.L. Rogach, Semiconductor nanocrystals emitting in the second near-infrared window: optical properties and application in biomedical imaging, *Adv. Opt. Mater.* 10 (2022), 2200226.
- [6] C. Zhu, Z. Chen, S. Gao, B.L. Goh, I.B. Samsudin, K.W. Lwe, Y. Wu, C. Wu, X. Su, Recent advances in non-toxic quantum dots and their biomedical applications, *Prog. Nat. Sci.* 29 (2019) 628–640.
- [7] M.J. Fang, C.W. Tsao, Y.J. Hsu, Semiconductor nanoheterostructures for photoconversion applications, *J. Phys. D.* 53 (2020), 143001.
- [8] M. Tan, F. Li, N. Cao, H. Li, X. Wang, C. Zhang, D. Jaque, G. Chen, Accurate in vivo nanothermometry through NIR-II lanthanide luminescence lifetime, *Small* 16 (2020), e2004118.
- [9] F. Ding, Y. Zhan, X. Lu, Y. Sun, Recent advances in near-infrared II fluorophores for multifunctional biomedical imaging, *Chem. Sci.* 9 (2018) 4370–4380.
- [10] B. del Rosal, D. Ruiz, I. Chaves-Coira, B.H. Juárez, L. Monge, G. Hong, N. Fernández, D. Jaque, In vivo contactless brain nanothermometry, *Adv. Funct. Mater.* 28 (2018), 1806088.
- [11] E. Ximendes, R. Marin, Y. Shen, D. Ruiz, D. Gomez-Cerezo, P. Rodriguez-Sevilla, J. Lifante, P.X. Viveros-Mendez, F. Gamez, D. Garcia-Soriano, G. Salas, C. Zalbidea, A. Espinosa, A. Benayas, N. Garcia-Carrillo, L. Cusso, M. Desco, F. J. Teran, B.H. Juarez, D. Jaque, Infrared-emitting multimodal nanostructures for controlled in vivo magnetic hyperthermia, *Adv. Mater.* 33 (2021), e2100077.
- [12] J. Lifante, Y. Shen, I. Zabala Gutierrez, I. Rubia-Rodriguez, D. Ortega, N. Fernandez, S. Melle, M. Granado, J. Rubio-Retama, D. Jaque, E. Ximendes, Reaching deeper: absolute in vivo thermal reading of liver by combining superbright Ag₂S nanothermometers and in silico simulations, *Adv. Sci.* 8 (2021), 2003838.
- [13] I.Z. Gutierrez, C. Gerke, Y. Shen, E. Ximendes, M.M. Silvan, R. Marin, D. Jaque, O. G. Calderon, S. Melle, J. Rubio-Retama, Boosting the near-infrared emission of Ag₂S nanoparticles by a controllable surface treatment for bioimaging applications, *ACS Appl. Mater. Interfaces* 14 (2022) 4871–4881.
- [14] X. Yang, Z. Wang, H. Huang, S. Ling, R. Zhang, Y. Zhang, G. Chen, C. Li, Q. Wang, A targeted activatable NIR-IIb nanoprobe for highly sensitive detection of ischemic stroke in a photothrombotic stroke model, *Adv. Healthc. Mater.* 10 (2021), e2001544.
- [15] H. He, Y. Lin, Z.Q. Tian, D.L. Zhu, Z.L. Zhang, D.W. Pang, Ultrasmall Pb:Ag(2)S quantum dots with uniform particle size and bright tunable fluorescence in the NIR-II window, *Small* 14 (2018), e1703296.
- [16] J. Cao, H. Zhu, D. Deng, B. Xue, L. Tang, D. Mahounga, Z. Qian, Y. Gu, In vivo NIR imaging with PbS quantum dots entrapped in biodegradable micelles, *J. Biomed. Mater. Res.* 100 (2012) 958–968.
- [17] L.C. Spangler, L. Lu, C.J. Kiely, B.W. Berger, S. McIntosh, Biomimetic mineralization of PbS and PbS–CdS core-shell nanocrystals and their application in quantum dot sensitized solar cells, *J. Mater. Chem.* 4 (2016) 6107–6115.
- [18] P. Jiang, R. Wang, Z. Chen, Thiol-based non-injection synthesis of near-infrared Ag₂S/ZnS core/shell quantum dots, *RSC Adv.* 5 (2015) 56789–56793.
- [19] W. Ouyang, J. Sun, Biosynthesis of silver sulfide quantum dots in wheat endosperm cells, *Mater. Lett.* 164 (2016) 397–400.
- [20] Y. Shen, J. Lifante, E. Ximendes, H.D.A. Santos, D. Ruiz, B.H. Juarez, I. Zabala Gutierrez, V. Torres Vera, J. Rubio Retama, E. Martin Rodriguez, D.H. Ortgies, D. Jaque, A. Benayas, B. Del Rosal, Perspectives for Ag(2)S NIR-II nanoparticles in biomedicine: from imaging to multifunctionality, *Nanoscale* 11 (2019) 19251–19264.
- [21] Y. Chen, L. Xue, Q. Zhu, Y. Feng, M. Wu, Recent advances in second near-infrared region (NIR-II) fluorophores and biomedical applications, *Front. Chem.* 9 (2021), 750404.
- [22] Y. Zhang, G. Hong, Y. Zhang, G. Chen, F. Li, H. Dai, Q. Wang, Ag₂S quantum dot: a bright and biocompatible fluorescent nanoprobe in the second near-infrared window, *ACS Nano* 6 (2012) 3695–3702.
- [23] X.L. Ge, B. Huang, Z.L. Zhang, X. Liu, M. He, Z. Yu, B. Hu, R. Cui, X.J. Liang, D. W. Pang, Glucose-functionalized near-infrared Ag₂Se quantum dots with renal excretion ability for long-term in vivo tumor imaging, *J. Mater. Chem. B* 7 (2019) 5782–5788.
- [24] A. Skripka, D. Mendez-Gonzalez, R. Marin, E. Ximendes, B. Del Rosal, D. Jaque, P. Rodriguez-Sevilla, Near infrared bioimaging and biosensing with semiconductor and rare-earth nanoparticles: recent developments in multifunctional nanomaterials, *Nanoscale Adv.* 3 (2021) 6310–6329.
- [25] A.M. Saeboe, A.Y. Nikiforov, R. Toufanian, J.C. Kays, M. Chern, J.P. Casas, K. Han, A. Piryatinski, D. Jones, A.M. Dennis, Extending the near-infrared emission range of indium phosphide quantum dots for multiplexed, *Nano Lett.* 21 (2021) 3271–3279.
- [26] L.M. Nieves, J.C. Hsu, K.C. Lau, A.D.A. Maidment, D.P. Cormode, Silver telluride nanoparticles as biocompatible and enhanced contrast agents for X-ray imaging: an in vivo breast cancer screening study, *Nanoscale* 13 (2021) 163–174.
- [27] Y.W. Liu, D.K. Ko, S.J. Oh, T.R. Gordon, V. Doan-Nguyen, T. Paik, Y. Kang, X. Ye, L. Jin, C.R. Kagan, C.B. Murray, Near-infrared absorption of monodisperse silver telluride (Ag₂Te) nanocrystals and photoconductive response of their self-assembled superlattices, *Chem. Mater.* 23 (2011) 4657–4659.
- [28] A. Sahu, A. Khare, D.D. Deng, D.J. Norris, Quantum confinement in silver selenide semiconductor nanocrystals, *Chem. Commun.* 48 (2012) 5458–5460.
- [29] D. Cadavid, M. Ibáñez, A. Shavel, O.J. Durá, M.A. López de la Torre, A. Cabot, Organic ligand displacement by metal salts to enhance nanoparticle functionality: thermoelectric properties of Ag₂Te, *J. Mater. Chem.* 1 (15) (2013) 4864–4870.
- [30] Y.P. Gu, R. Cui, Z.L. Zhang, Z.X. Xie, D.W. Pang, Ultrasmall near-infrared Ag₂Se quantum dots with tunable fluorescence for in vivo imaging, *J. Am. Chem. Soc.* 134 (2012) 79–82.
- [31] A.M. Smith, M.C. Mancini, S. Nie, Second window for in vivo imaging, *Nat. Nanotechnol.* 4 (2009) 710–711.
- [32] G. Hong, S. Diao, A.L. Antaris, H. Dai, Carbon nanomaterials for biological imaging and nanomedicinal therapy, *Chem. Rev.* 115 (2015) 10816–10906.
- [33] J.J. Zhang, Y. Lin, H. Zhou, H. He, J.J. Ma, M.Y. Luo, Z.L. Zhang, D.W. Pang, Cell membrane-camouflaged NIR II fluorescent Ag(2)Te quantum dots-based nanoprobes for enhanced in vivo homotypic tumor imaging, *Adv. Healthc. Mater.* 8 (2019), e1900341.
- [34] L.J. Shi, C.N. Zhu, H. He, D.L. Zhu, Z.L. Zhang, D.W. Pang, Z.Q. Tian, Near-infrared Ag₂Se quantum dots with distinct absorption features and high fluorescence quantum yields, *RSC Adv.* 6 (2016) 38183–38186.
- [35] H.D.A. Santos, I. Zabala Gutierrez, Y. Shen, J. Lifante, E. Ximendes, M. Laurenti, D. Mendez-Gonzalez, S. Melle, O.G. Calderon, E. Lopez Cabarcos, N. Fernandez, I. Chaves-Coira, D. Lucena-Agell, L. Monge, M.D. Mackenzie, J. Marques-Hueso, C.M.S. Jones, C. Jacinto, B. Del Rosal, A.K. Kar, J. Rubio-Retama, D. Jaque, Ultrafast photochemistry produces superbright short-wave infrared dots for low-dose in vivo imaging, *Nat. Commun.* 11 (1) (2020) 2933.
- [36] H. Yang, R. Li, Y. Zhang, M. Yu, Z. Wang, X. Liu, W. You, D. Tu, Z. Sun, R. Zhang, X. Chen, Q. Wang, Colloidal alloyed quantum dots with enhanced photoluminescence quantum yield in the NIR-II window, *J. Am. Chem. Soc.* 143 (2021) 2601–2607.
- [37] Z. Wang, T. Gu, T. Kadohira, T. Tada, S. Watanabe, Migration of Ag in low-temperature Ag₂S from first principles, *J. Chem. Phys.* 128 (2008), 014704.
- [38] M.A. Hamilton, A.C. Barnes, W.S. Howells, H.E. Fischer, Ag⁺ dynamics in the superionic and liquid phases of Ag₂Se and Ag₂Te by coherent quasi-elastic neutron scattering, *J. Phys. Condens. Matter* 13 (2001) 2425.
- [39] Y. Du, B. Xu, T. Fu, M. Cai, F. Li, Y. Zhang, Q. Wang, Near-infrared photoluminescent Ag₂S quantum dots from a single source precursor, *J. Am. Chem. Soc.* 132 (2010) 1470–1471.
- [40] P. Li, Q. Peng, Y. Li, Controlled synthesis and self-assembly of highly monodisperse Ag and Ag(2)S nanocrystals, *Chemistry* 17 (2011) 941–946.
- [41] L. Chen, G. Li, Functions of 1-dodecanethiol in the synthesis and post-treatment of copper sulfide nanoparticles relevant to their photocatalytic applications, *ACS Appl. Nano Mater.* 1 (2018) 4587–4593.
- [42] S.I. Sadovnikov, A.I. Gusev, Recent progress in nanostructured silver sulfide: from synthesis and nonstoichiometry to properties, *J. Mater. Chem.* 5 (2017) 17676–17704.
- [43] A. Ortega-Rodriguez, Y. Shen, I. Zabala Gutierrez, H.D.A. Santos, V. Torres Vera, E. Ximendes, G. Villaverde, J. Lifante, C. Gerke, N. Fernandez, O.G. Calderon, S. Melle, J. Marques-Hueso, D. Mendez-Gonzalez, M. Laurenti, C.M.S. Jones, J. M. Lopez-Romero, R. Contreras-Caceres, D. Jaque, J. Rubio-Retama, 10-Fold quantum yield improvement of Ag₂S nanoparticles by fine compositional tuning, *ACS Appl. Mater. Interfaces* 12 (2020) 12500–12509.

- [44] W.P. Lim, Z. Zhang, H.Y. Low, W.S. Chin, Preparation of Ag₂S nanocrystals of predictable shape and size, *Angew. Chem. Int. Ed.* 116 (2004) 5803–5807.
- [45] Y.R. Luo, J.A. Kerr, Bond dissociation energies, *CRC Handb. Chem. Phys.* 89 (2012) 89.
- [46] M. Yarema, S. Pochler, M. Sytnyk, R. Seyrkammer, R.T. Lechner, G. Fritz-Popovski, D. Jarzab, K. Szendrei, R. Resel, O. Korovyanko, M.A. Loi, O. Paris, G. Hesser, W. Heiss, Infrared emitting and photoconducting colloidal silver chalcogenide nanocrystal quantum dots from a silylamide-promoted synthesis, *ACS Nano* 5 (2011) 3758–3765.
- [47] Z.Y. Liu, A.A. Liu, H. Fu, Q.Y. Cheng, M.Y. Zhang, M.M. Pan, L.P. Liu, M.Y. Luo, B. Tang, W. Zhao, J. Kong, X. Shao, D.W. Pang, Breaking through the size control dilemma of silver chalcogenide quantum dots via trialkylphosphine-induced ripening: leading to Ag(2)Te emitting from 950 to 2100 nm, *J. Am. Chem. Soc.* 143 (2021) 12867–12877.
- [48] M.Y. Zhang, A.A. Liu, H. Fu, W. Zhang, S.H. Zhang, Z.Y. Liu, L.H. Jiang, X. Shao, D.W. Pang, Regulation of silver precursor reactivity via tertiary phosphine to synthesize near-infrared Ag₂Te with photoluminescence quantum yield of up to 14.7, *Chem. Mater.* 33 (2021) 9524–9533.
- [49] B.C. Fitzmorris, Y.C. Pu, J.K. Cooper, Y.F. Lin, Y.J. Hsu, Y. Li, J.Z. Zhang, Optical properties and exciton dynamics of alloyed core/shell Cd_(1-x)Zn_xSe/ZnSe/ZnS quantum dots, *ACS Appl. Mater. Interfaces* 5 (2013) 2893–2900.
- [50] Y. Zheng, Z. Yang, J.Y. Ying, Aqueous synthesis of glutathione-capped ZnSe and Zn_{1-x}Cd_xSe alloyed quantum dots, *Adv. Mater.* 19 (2007) 1475–1479.
- [51] M.H. Xinhua Zhong, Zhili Dong, Timothy J. White, Wolfgang Knoll, Composition-tunable Zn_xCd_{1-x}Se nanocrystals with high luminescence and stability, *J. Am. Chem. Soc.* 125 (2003) 8589–8594.
- [52] G.X. Liang, M.M. Gu, J.R. Zhang, J.J. Zhu, Preparation and bioapplication of high-quality, water-soluble, biocompatible, and near-infrared-emitting CdSeTe alloyed quantum dots, *Nanotechnology* 20 (2009), 415103.
- [53] H. Qian, L. Li, J. Ren, One-step and rapid synthesis of high quality alloyed quantum dots (CdSe–CdS) in aqueous phase by microwave irradiation with controllable temperature, *Mater. Res. Bull.* 40 (2005) 1726–1736.
- [54] J. Zhang, Q. Yang, H. Cao, C.I. Ratcliffe, D. Kingston, Q.Y. Chen, J. Ouyang, X. Wu, D.M. Leek, F.S. Riehle, K. Yu, Bright gradient-alloyed CdSe_{0.8}S_{0.2} quantum dots exhibiting cyan-blue emission, *Chem. Mater.* 28 (2016) 618–625.
- [55] Z. Sun, C. Liu, H. Yang, X. Yang, Y. Zhang, H. Lin, Y. Li, Q. Wang, AgAuSe quantum dots with absolute photoluminescence quantum yield of 87.2%: the effect of capping ligand chain length, *Nano Res.* 15 (2022) 8555–8563.
- [56] J.H. Kim, B.Y. Kim, E.P. Jang, S.Y. Yoon, K.H. Kim, Y.R. Do, H. Yang, Synthesis of widely emission-tunable Ag–Ga–S and its quaternary derivative quantum dots, *Chem. Eng. J.* 347 (2018) 791–797.
- [57] J. Song, C. Ma, W. Zhang, X. Li, W. Zhang, R. Wu, X. Cheng, A. Ali, M. Yang, L. Zhu, R. Xia, X. Xu, Bandgap and structure engineering via cation exchange: from binary Ag₂S to ternary AgInS₂, quaternary AgZnInS alloy and AgZnInS/ZnS core/shell fluorescent nanocrystals for bioimaging, *ACS Appl. Mater. Interfaces* 8 (2016) 24826–24836.
- [58] Y. Shu, J. Yan, Q. Lu, Z. Ji, D. Jin, Q. Xu, X. Hu, Pb ions enhanced fluorescence of Ag₂S QDs with tunable emission in the NIR-II window: facile one pot synthesis and their application in NIR-II fluorescent bio-sensing, *Sensor. Actuator. B Chem.* 307 (2020), 127539.
- [59] M. Yu, X. Yang, Y. Zhang, H. Yang, H. Huang, Z. Wang, J. Dong, R. Zhang, Z. Sun, C. Li, Q. Wang, Pb-doped Ag₂Se quantum dots with enhanced photoluminescence in the NIR-II window, *Small* 17 (2021), e2006111.
- [60] H. Yang, H. Huang, X. Ma, Y. Zhang, X. Yang, M. Yu, Z. Sun, C. Li, F. Wu, Q. Wang, Au-doped Ag(2) Te quantum dots with bright NIR-IIb fluorescence for in situ monitoring of angiogenesis and arteriogenesis in a hindlimb ischemic model, *Adv. Mater.* 33 (2021), e2103953.
- [61] J. Dana, P. Maity, H.N. Ghosh, Hot-electron transfer from the semiconductor domain to the metal domain in CdSe@CdSAu nano-heterostructures, *Nanoscale* 9 (2017) 9723–9731.
- [62] X. Zhang, W. Wang, L. Su, X. Ge, J. Ye, C. Zhao, Y. He, H. Yang, J. Song, H. Duan, Plasmonic-fluorescent janus Ag/Ag(2)S nanoparticles for in situ H(2)O(2)-activated NIR-II fluorescence imaging, *Nano Lett.* 21 (2021) 2625–2630.
- [63] P. Lin, J. Shi, L. Ming, Y. Sheng, L. Song, M. Hong, Y. Zhang, An intelligent persistent luminescence nanoplatfrom with high-efficiency O₂ utilization for continuous hypoxic tumors treatment, *Chem. Eng. J.* 442 (2022), 135638.
- [64] B. Lin, H. Chen, D. Liang, W. Lin, X. Qi, H. Liu, X. Deng, Acidic pH and high-H(2) O(2) dual tumor microenvironment-responsive nanocatalytic graphene oxide for cancer selective therapy and recognition, *ACS Appl. Mater. Interfaces* 11 (2019) 11157–11166.
- [65] C. Zhang, L. Yan, X. Wang, X. Dong, R. Zhou, Z. Gu, Y. Zhao, Tumor microenvironment-responsive Cu(2)(OH)PO(4) nanocrystals for selective and controllable radiosensitization via the X-ray-triggered fenton-like reaction, *Nano Lett.* 19 (2019) 1749–1757.
- [66] J. Ye, Z. Li, Q. Fu, Q. Li, X. Zhang, L. Su, H. Yang, J. Song, Quantitative photoacoustic diagnosis and precise treatment of inflammation in vivo using activatable theranostic nanoprobe, *Adv. Funct. Mater.* 30 (2020), 2001771.
- [67] R. Marin, A. Benayas, N. García-Carillo, J. Lifante, J. Yao, D. Mendez-Gonzalez, F. Sanz-Rodríguez, J. Rubio-Retama, L.V. Besteiro, D. Jaque, Nanoprobes for biomedical imaging with tunable near-infrared optical properties obtained via green synthesis, *Adv. Photonics Res.* 3 (2021), 210026.
- [68] T.G. Kim, D. Zherebetskyy, Y. Bekenstein, M.H. Oh, L.W. Wang, E. Jang, A. P. Alivisatos, Trap passivation in indium-based quantum dots through surface fluorination: mechanism and applications, *ACS Nano* 12 (2018) 11529–11540.
- [69] Y. Sung, W. Lee, E. Lee, Y.H. Ko, S. Kim, Ion-pair ligand-assisted surface stoichiometry control of Ag₂S nanocrystals, *Chem. Mater.* 34 (2022) 9945–9954.
- [70] D. Ruiz, B. del Rosal, M. Acebrón, C. Palencia, C. Sun, J. Cabanillas-González, M. López-Haro, A.B. Hungria, D. Jaque, B.H. Juarez, Ag/Ag₂S nanocrystals for high sensitivity near-infrared luminescence nanothermometry, *Adv. Funct. Mater.* 27 (2017), 1604629.
- [71] G. Hong, J.T. Robinson, Y. Zhang, S. Diao, A.L. Antaris, Q. Wang, H. Dai, In vivo fluorescence imaging with Ag₂S quantum dots in the second near-infrared region, *Angew. Chem. Int. Ed.* 51 (2012) 9818–9821.
- [72] C. Bullen, P. Mulvaney, The effects of chemisorption on the luminescence of CdSe quantum dots, *Langmuir* 22 (2006) 3007–3013.
- [73] V.I. Bukhtiyarov, M.G. Slin'ko, Metallic nanosystems in catalysis, *Russ. Chem. Rev.* 70 (2) (2001) 147–159.
- [74] Y.R. Luo, J.A. Kerr, physics, Bond dissociation energies, *CRC Handb. Chem. Phys.* 89 (2012) 89.
- [75] O.I. Micic, J. Sprague, Z. Lu, A.J. Nozik, Highly efficient band-edge emission from InP quantum dots, *Appl. Phys. Lett.* 68 (1996) 3150–3152.
- [76] S. Adam, D.V. Talapin, H. Borchert, A. Lobo, C. McGinley, A.R.B. De Castro, M. Haase, H. Weller, T. Moller, The effect of nanocrystal surface structure on the luminescence properties: photoemission study of HF-etched InP nanocrystals, *J. Chem. Phys.* 123 (2005), 084706.
- [77] T.G. Kim, D. Zherebetskyy, Y. Bekenstein, M. Oh, A.P. Alivisatos, Trap passivation in indium-based quantum dots through surface fluorination: mechanism and applications, *ACS Nano* 12 (2018) 11529–11540.
- [78] D.V. Talapin, N. Gaponik, H. Borchert, A.L. Rogach, H. Weller, Etching of colloidal InP nanocrystals with fluorides: photochemical nature of the process resulting in high photoluminescence efficiency, *ChemInform* 34 (2003) 12659–12663.
- [79] R.F. Ubbink, G. Almeida, H. Iziyi, F. Indy du, R. Verkleij, S. Ganapathy, E.R.H. V. Eck, A.J. Houtepen, A water-free in situ hf treatment for ultrabright inq quantum dots, *Chem. Mater.* 34 (2022) 10093–10103.
- [80] M. Peterson, L. Cass, R. Harris, K. Edme, K. Sung, E. Weiss, The role of ligands in determining the exciton relaxation dynamics in semiconductor quantum dots, *Annu. Rev. Phys. Chem.* 65 (2014) 317–399.
- [81] A.M. Munro, D.S. Ginger, Photoluminescence quenching of single CdSe nanocrystals by ligand adsorption, *Nano Lett.* 8 (2008) 2585–2590.
- [82] S. Wuister, A.F.M. Donega, A. Meijerink, Influence of thiol capping on the exciton luminescence and decay kinetics of CdTe and CdSe quantum dots, *J. Phys. Chem. B* 108 (2004) 17393–17397.
- [83] M.J. Turo, J.E. Macdonald, Crystal-bound vs surface-bound thiols on nanocrystals, *ACS Nano* 8 (2014) 10205–10213.
- [84] X. Peng, M.C. Schlamp, A.V. Kadavanich, A.P. Alivisatos, Epitaxial growth of highly luminescent CdSe/CdS core/shell nanocrystals with photostability and electronic accessibility, *J. Am. Chem. Soc.* 119 (1997) 7019–7029.
- [85] R.B. Little, M.A. El-Sayed, G.W. Bryant, S. Burke, Formation of quantum-dot quantum-well heterostructures with large lattice mismatch: ZnS/CdS/ZnS, *J. Chem. Phys.* 114 (2001) 1813–1822.
- [86] P. Reiss, M. Protiere, L. Li, Core/shell semiconductor nanocrystals, *Small* 5 (2009) 154–168.
- [87] A. Sahu, D. Kumar, Core-shell quantum dots: a review on classification, materials, application, and theoretical modeling, *J. Alloys Compd.* 924 (2022), 166508.
- [88] D. Vasudevan, R.R. Gaddam, A. Trinch, I. Cole, Core-shell quantum dots: properties and applications, *J. Alloys Compd.* 636 (2015) 395–404.
- [89] Y. Jang, A. Shapiro, M. Isarov, A. Rubin-Brusilovski, A. Safran, A.K. Budniak, F. Horani, J. Dehnell, A. Sashchiuk, E. Lifshitz, Interface control of electronic and optical properties in IV–VI and II–VI core/shell colloidal quantum dots: a review, *Chem. Commun.* 53 (2017) 1002–1024.
- [90] O. Ovchinnikov, A. Perepelitsa, M. Smirnov, A. Latyshev, I.G. Grevtseva, R. B. Vasiliev, G.N. Goltsman, A.G. Vitukhnovsky, Luminescence of colloidal Ag₂S/ZnS core/shell quantum dots capped with thioglycolic acid, *J. Lumin.* 220 (2020), 117008.
- [91] Y.M. Zeng, L.J. Pan, J. Wang, Y.L. Fan, Y. Shu, D.W. Pang, Z.L.J.C. Zhang, Interfacial synthesis of Ag₂S/ZnS core/shell quantum dots in a droplet microreactor, *ChemistrySelect* 5 (2020) 5889–5894.
- [92] C. Chen, X. He, L. Gao, N.J.A.a.m. Ma, interfaces, Cation exchange-based facile aqueous synthesis of small, stable, and nontoxic near-infrared Ag₂Te/ZnS core/shell quantum dots emitting in the second biological window, *ACS Appl. Mater. Interfaces* 5 (2013) 1149–1155.
- [93] L. Li, A. Pandey, D.J. Werder, B.P. Khanal, J.M. Pietryga, V.I. Klimov, Efficient synthesis of highly luminescent copper indium sulfide-based core/shell nanocrystals with surprisingly long-lived emission, *J. Am. Chem. Soc.* 133 (2011) 1176–1179.
- [94] S. Shen, Y. Zhang, Y. Liu, L. Peng, X. Chen, Q. Wang, Manganese-doped Ag₂S–ZnS heteronanostructures, *Chem. Mater.* 24 (2012) 2407–2413.
- [95] S. Shen, Y. Zhang, L. Peng, Y. Du, Q. Wang, Matchstick-shaped Ag₂S–ZnS heteronanostructures preserving both UV/blue and near-infrared photoluminescence, *Angew. Chem.* 50 (2011) 7115–7118.
- [96] Y. Zhang, H. Yang, X. An, Z. Wang, X. Yang, M. Yu, R. Zhang, Z. Sun, Q.J.S. Wang, Controlled synthesis of Ag₂Te@ Ag₂S core-shell quantum dots with enhanced and tunable fluorescence in the second near-infrared window, *Small* 16 (2020), 2001003.
- [97] A.K. Patnaik, I. Adamovich, J.R. Gord, S. Roy, Recent advances in ultrafast-laser-based spectroscopy and imaging for reacting plasmas and flames, *Plasma Sources Sci. Technol.* 26 (2017), 103001.
- [98] L. Jiang, A.D. Wang, B. Li, T.H. Cui, Y.F. Lu, Electrons dynamics control by shaping femtosecond laser pulses in micro/nanofabrication: modeling, method, measurement and application, *Light Sci. Appl.* 7 (2018), 17134.

- [99] K. Sugioka, Progress in ultrafast laser processing and future prospects, *Nanophotonics* 6 (2017) 393–413.
- [100] M. Malinauskas, A. Zukauskas, S. Hasegawa, Y. Hayasaki, V. Mizeikis, R. Buividas, S. Juodkazis, Ultrafast laser processing of materials: from science to industry, *Light Sci. Appl.* 5 (2016), e16133.
- [101] B. Zhang, L. Wang, F. Chen, Recent advances in femtosecond laser processing of LiNbO_3 crystals for photonic applications, *Laser Photon. Rev.* 14 (2020), 1900407.
- [102] B. Zhang, D. Tan, X. Liu, L. Tong, P.G. Kazansky, J. Qiu, Self-organized periodic crystallization in unconventional glass created by an ultrafast laser for optical attenuation in the broadband near-infrared region, *Adv. Opt. Mater.* 7 (2019), 1900593.
- [103] I. Miyamoto, H. Lubatschowski, K.F. Kobayashi, A. Heisterkamp, F. Will, K. Sugioka, R. Poprawe, A.I. Singh, J. Serbin, H. Helvajian, A. Ostendorf, O. Kermani, R. Heermann, H. Welling, W. Ertmer, Medical and biological applications for ultrafast laser pulses, third international symposium on laser precision microfabrication, *Proc. SPIE* 4830 (2003) 537–543.
- [104] C.L. Hoy, O. Ferhanoglu, M. Yildirim, K. Ki Hyun, S.S. Karajanagi, K.M.C. Chan, J. B. Kobler, S.M. Zeitels, A. Ben-Yakar, Clinical ultrafast laser surgery: recent advances and future directions, *IEEE J. Sel. Top. Quant.* 20 (2014) 242–255.
- [105] R. Srinivasan, E. Sutcliffe, B. Braren, Ablation and etching of polymethylmethacrylate by very short (160 fs) ultraviolet (308 nm) laser pulses, *Appl. Phys. Lett.* 51 (1987) 1285–1287.
- [106] S. Kupper, M. Stuke, Femtosecond uv excimer laser ablation, *Appl. Phys. B* 44 (1987) 199–204.
- [107] K. Sugioka, Y. Cheng, Ultrafast lasers-reliable tools for advanced materials processing, *Light Sci. Appl.* 3 (2014) e149–e149.
- [108] R. Stoian, J.P. Colombier, Advances in ultrafast laser structuring of materials at the nanoscale, *Nanophotonics* 9 (2020) 4665–4688.
- [109] D. Zhu, J. Yan, J. Xie, Z. Liang, H. Bai, Ultrafast laser-induced atomic structure transformation of Au nanoparticles with improved surface activity, *ACS Nano* 15 (2021) 13140–13147.
- [110] V. Nguyen, L. Yan, N. Zhao, N. Van Canh, N.T.N. Hang, P.H. Le, Tuning photoluminescence of boron nitride quantum dots via surface functionalization by femtosecond laser ablation, *J. Mol. Struct.* 1244 (2021), 130922.